Density of hydrophobically confined deeply cooled water investigated by small angle X-ray scattering

Kao-Hsiang Liu, Yang Zhang, U-Ser Jeng, and Chung-Yuan Mou

Citation: The Journal of Chemical Physics **143**, 094704 (2015); doi: 10.1063/1.4929843
View online: https://doi.org/10.1063/1.4929843
View Table of Contents: http://aip.scitation.org/toc/jcp/143/9
Published by the American Institute of Physics

Articles you may be interested in

Density and anomalous thermal expansion of deeply cooled water confined in mesoporous silica investigated by synchrotron X-ray diffraction
The Journal of Chemical Physics **139**, 064502 (2013); 10.1063/1.4817186

Single particle dynamics of water confined in a hydrophobically modified MCM-41-S nanoporous matrix
The Journal of Chemical Physics **130**, 134512 (2009); 10.1063/1.3097800

PHYSICS TODAY
WHITEPAPERS

ADVANCED LIGHT CURE ADHESIVES

Take a closer look at what these environmentally friendly adhesive systems can do

READ NOW

PRESENTED BY
MASTERBOND
ADHESIVES | SEALANTS | COATINGS

THE JOURNAL OF CHEMICAL PHYSICS **143**, 094704 (2015)

Density of hydrophobically confined deeply cooled water investigated by small angle X-ray scattering

Kao-Hsiang Liu,[1,2,a)] Yang Zhang,[3] U-Ser Jeng,[4] and Chung-Yuan Mou[1]
[1] *Department of Chemistry, National Taiwan University, Taipei 10617, Taiwan*
[2] *Joint Institute for Neutron Science, Oak Ridge National Laboratory, Oak Ridge, Tennessee 37831, USA*
[3] *Department of Nuclear, Plasma, and Radiological Engineering, University of Illinois at Urbana-Champaign, Urbana, Illinois 61801, USA*
[4] *National Synchrotron Radiation Research Center, Hsinchu 30076, Taiwan*

(Received 29 May 2015; accepted 19 August 2015; published online 3 September 2015)

Water's behavior near hydrophobic surfaces has attracted great attention due to chemical and geological applications. Here, we report small angle X-ray scattering (SAXS) studies of water confined in the hydrophobic nanoporous carbon material, CMK-1-14, from ambient to deeply cooled temperatures. By monitoring the scattering intensity of the first Bragg peak, which is directly related to the scattering length density contrast between the carbon matrix and the confined water, the average density of the hydrophobically confined water was determined from 300 K to 150 K at ambient pressure. Furthermore, differential scanning calorimetry and X-ray diffraction measurements showed that the majority of such hydrophobically confined water did not crystallize in the investigated temperature range. By exploiting the fast speed of SAXS measurements and the continuous temperature ramping, the average density profile and the deduced thermal expansion coefficient (α_p) were obtained. We found that the well-known density maximum of water at 277 K downshifted to 260 K, and the density minimum which has been observed in hydrophilic confinement disappeared. In addition, the previously measured large density decreasing of 18% at low temperature was recalibrated to a more reasonable 10% instead. Consequently, the recalculated α_p peak was found to be quite similar to that of the water confined in hydrophilic MCM-41-S-15 suggesting an intrinsic property of water, which does not sensitively depend on the confinement surface. © *2015 AIP Publishing LLC.* [http://dx.doi.org/10.1063/1.4929843]

I. INTRODUCTION

Water confined in nano-space plays a fundamental role in many aspects of biological,[1] geological, meteorological, and industrial fields. The water-surface interaction, hydrophilicity, and the geometry of the confinement alter the formation of the random hydrogen bond network and the overall energy landscape of the system.[2,3] Nanoscopic water, though small in size, could lead to critical consequences in many physicochemical processes. In life science, a few water molecules could control the folding structure of enzymes.[4,5] In civil engineering, a few layers of water determine the construction of cement.[6] From the point of view of fundamental science, nanoscopic waters are even more interesting at temperatures lower than the bulk freezing point.[7–10] The nucleation temperature of nano-confined water can be much lower than that of the bulk form. In some extreme cases, freezing can even be completely inhibited, allowing the study in the so-called "no man's land"[11] of liquid water. In this mysterious region, many conflicting theories have been proposed[12–16] and debated[17–20] to explain the anomalous thermodynamic response functions.[21,22] Both the structures and dynamics of the deeply cooled confined water have received tremendous attention recently.[23–27]

While there are numerous research efforts on hydrophilically confined water, the study of nanoscopic water under hydrophobic confinement is much less. In-depth understanding of the behavior of water near hydrophobic surfaces could shed some light on the interaction between the surface and confined water. Hydrophobic confinement may also allow extra room for manipulating the physical and chemical properties of confined water.[28] Along this line, the hydrophobic confined water has been recently studied in carbon nanotubes,[29,30] graphene,[31,32] hydrophobic modified silica matrix,[33] mesoporous carbon,[34] activated carbon fiber,[35] etc.

Yet, merely a handful of researches have aimed at the structure change of hydrophobically confined water over a large temperature range. A small angle neutron scattering (SANS) study by Zhang *et al.* measured the density as a function of temperature of H_2O confined in mesoporous carbon material, CMK-1-14, at very low temperatures.[36] By monitoring the intensity change of the Bragg peak, which is directly related to the contrast between the carbon matrix and the confined water, the average density of confined water was determined. The water density was assumed to be affected by the hydrophobic carbon wall hence gave a very different profile from the case in hydrophilic confinement. The density maximum was found to be downshifted to 260 K and the density minimum was absent down to 130 K. The deduced thermal expansion coefficient showed a much boarder peak

a)Author to whom correspondence should be addressed. Electronic mail: codeliu@gmail.com

 © 2015 AIP Publishing LLC

spanning from 240 K to 180 K. This is in contrast to the SANS results obtained for confined heavy water D_2O in nanoporous silica where density minimum at 210 K was found.[37]

One surprising result from the SANS measurements is that the obtained density of water at the low temperature end showed a huge reduction compared to density at room temperature. The authors hypothesized that it might indicate a wetting-dewetting transition. A small angle X-ray scattering instrument built at a synchrotron source provides high flux, high resolution measurements, and essentially has no incoherent scattering background. So that X-ray could provide complimentary information to the previous neutron scattering studies in this water research project. Futamura *et al.* investigated the density of water in the micropores of activated carbon fibers with small angle X-ray scattering. Due to the lack of ordered structure within activated carbon fibers, a Debye-Bueche analysis was used to derive the density profile. They also found a negative thermal expansion over a wide temperature range (20-277 K) and no density minimum.[35]

In our previous study, the density of water confined in hydrophilic periodical nanopores of MCM-41-S-15 was carefully measured by synchrotron X-ray diffraction.[38] The density maximum at 277 K and the minimum at 200 K were revealed. Also a peak at 230 K in the thermal expansion coefficient was derived and it was interpreted as the sign of crossing the "Widom line" which is emanated from a hypothetical liquid-liquid critical point at elevated pressure. In this paper, the similar X-ray diffraction method was used to measure the liquid water confined in ordered hydrophobic nanoporous carbon, CMK-1-14. With continuous temperature ramping, we provided a detailed average density profile as a function of temperature at ambient pressure. The thermal expansion coefficient was also deduced.

II. EXPERIMENTS

A. Material synthesis

The CMK-1-14 was synthesized by using mesoporous silica MCM-48-S (cubic, *Ia3d* symmetry, consisting of two disconnected interwoven 3D pore systems) as a hard template and sucrose as the carbon source (dehydrated by sulfuric acid). The MCM-48-S was synthesized by reacting preformed β-zeolite seeds (composed by tetraethylammonium hydroxide (TEAOH, Acros), sodium hydroxide (NaOH), and fumed silica (Sigma)) with cetyltrimethylammonium bromide solution (C_{16}TAB, Acros), then transferring the mixture into an autoclave at 150 °C for 6 h. After cooling down to room temperature, solid sample was collected by filtration, washed by water and ethanol, dried at 60 °C in air overnight, and then calcined at 540 °C for 8 h. The molar ratios of the reactants are SiO_2:NaOH:TEAOH:C_{16}TAB:H_2O = 1:0.075:0.285:0.204:226.46. Then, CMK-1-14 was made by sulfuric acid dehydration of loaded sucrose inside the pores of MCM-48-S mesoporous silica. The MCM-48-S powder was mixed with sucrose solution together with sulfuric acid, and slowly heated to 160 °C. The process was repeated twice to ensure a homogeneous but not overfilled carbon loading inside the silica template. The mass ratio of the reactants is MCM-48-S:sucrose:sulfuric acid = 1:2:0.22. Then the obtained powder was calcined at 900 °C for 6 h under nitrogen atmosphere for carbonization. After the silica template was removed by hydrogen fluoride (HF) solution, the black powder of CMK-1-14 was obtained. Since the MCM-48-S was used as template instead of traditional MCM-48, CMK-1-14 has much smaller pore size (Barret-Joyner-Halenda (BJH) pore size 14 Å, compared to regular CMK-1, which has a pore size around 30 Å).

The CMK-1-14 sample was then hydrated by exposing to water vapor in a closed container until a full hydration level of 0.84 mass fraction (mass of water/mass of dry CMK-1-14) was achieved.

B. Synchrotron X-ray scattering

The small angle X-ray scattering experiments were performed at beamline 23A1 of Taiwan Light Source (TLS) in National Synchrotron Radiation Research Center (NSRRC), Taiwan. The incident energy was 14 keV. The observable Q range was from 0.05 to 0.6 $Å^{-1}$ covered by MARCCD two dimensional detector. A dedicated designed liquid nitrogen cooling system (LNCS) was used as temperature controller. LNCS is capable to cool down to at least 150 K, and a slow, steady, continuous ramping of temperature is possible. The ramping rate can be set as slow as 1 K/min within the accuracy of ±0.2 K to ensure the system thermal equilibrium. The slow ramping rate can guarantee the thermal equilibrium of samples. The detector was operated in continuous mode. Each frame was exposed for 50 s, and read out for 10 s. This setup can obtain 1 K/frame. When using LNCS, the samples were tightly packed and sealed in alumina pans. The pans were punched holes at both sides and sealed with Kapton films to allow X-ray passing through.

The wide angle X-ray diffraction experiments were performed in beamline 17A1 of TLS in NSRRC. The energy was fixed at 9.297 keV and giving the wavelength of 1.3336 Å. The 2θ range was covered from 2° to 40° by MAR 3450 on-line image plate scanner.

III. RESULTS AND DISCUSSION

The CMK-1-14 is composed of amorphous carbon; thus, its surface is uniformly hydrophobic. Nevertheless, CMK-1-14 still can be hydrated by water vapor without pressurized. This feature makes CMK-1-14 suitable for the water/hydrophobic surface interaction researches. With the BJH analysis,[39] we found the pore volume and the pore diameter to be 0.84 cm^3/g and 14 Å, respectively. One should notice that the pore size determined by BJH method is known to be underestimated, especially in such a small pore system. So the 14 Å is a nominal pore size and only for the convenience of comparing to similar materials.

The careful loading to avoid external water was achieved by taking water vapor adsorption isotherm (Figure 1). It is a type V adsorption isotherm, showing the low affinity between water vapor and the hydrophobic carbon surface of CMK-1-14. A very low adsorbed quantity shows at the relative pressure (P/P_0, P_0 is the saturated vapor pressure) below 0.55.

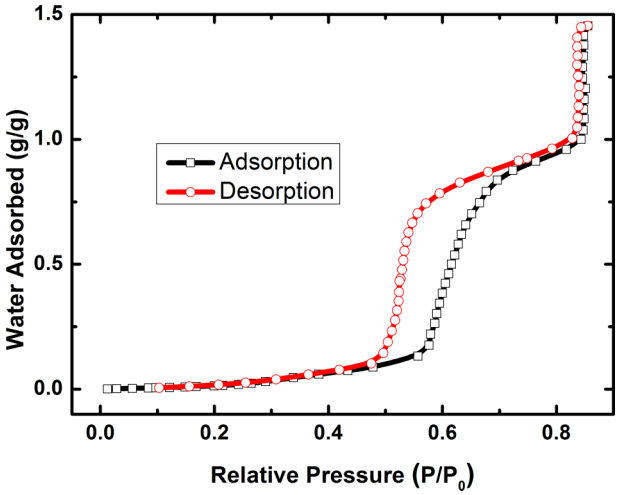

FIG. 1. Water vapor sorption isotherms of CMK-1-14 at 298 K. The hydrophobic surface can be seen as the type V isotherms.

The water condensed at the P/P_0 of about 0.55-0.7 into the nanopores. There was no further condensation in the range of $0.7 < P/P_0 < 0.8$. So we can be sure water loaded inside the nanopores by controlling the relative pressure of water vapor was in the range of 0.7–0.8. The hydration water amount can be measured precisely by thermogravimetric analysis. The amount of hydration water concurred with the BJH pore volume if the density of hydrated water was assumed to be 1.00 g/cm^3. Above the P/P_0 of 0.85, water condensed again in the inter-particle space, which is unwanted overfilled water. This helped us to realize the water vapor pressure necessary for capillary condensation, but low enough to avoid condensation on external surface. Water outside the pores would not affect the contrast between carbon matrix and internal water, therefore our method is still valid even if there is small amount of external water.

Figure 2 shows both the cooling and heating DSC scans of hydrated CMK-1-14. The scans were repeated twice and matched each other well. No significant melting/freezing peaks were detected. The small bumps at around 230 K in differential scanning calorimetry (DSC) scan can be assigned to the freezing of a small amount of expelled water into ice I_c at the openings of the carbon nanopores. The small latent heat indicated that the majority of water inside the pores did not freeze in the studied temperature range down to 130 K. More evidence is shown in the following X-ray diffarction (XRD) results.

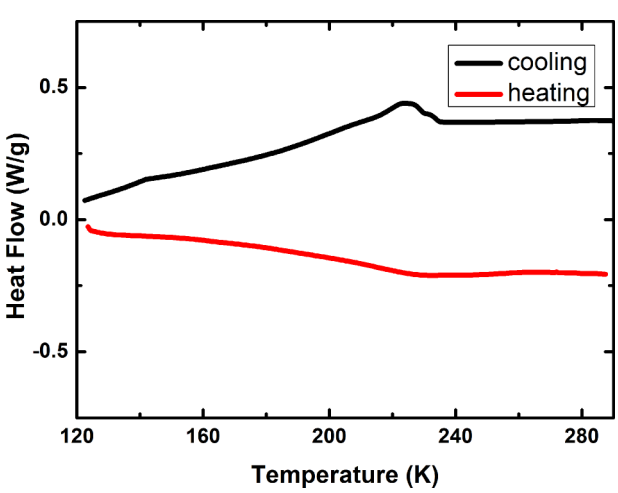

FIG. 2. The DSC scans of hydrated CMK-1-14. The scan rates were 5 K/min at both cooling and heating directions.

The *in situ* XRD of hydrated CMK-1-14 of cooling and heating scans is shown in Figures 3(a) and 3(b), respectively. The scattering angle $2\theta = 18°$-$26°$, was focused on the oxygen-oxygen arrangements of adsorbed water/ice structures. In Figure 3(a), there is only a very broad peak centered on $2\theta = 22°$ at 300 K, which came from the liquid water. Three sharp peaks appeared when the temperature decreased to about 260 K, and gradually grew as cooling. These three peaks can be assigned to ice I_h. At around 230 K, another broad peak appears at 20.94°. This broad peak can be assigned to ice I_c structure. In Figure 3(b), the reverse process was observed during the heating cycle. The broad ice I_c peak first melted at about 240 K, then the three ice I_h peaks melted at about 260 K. Above that temperature, the XRD patterns went back to a very broad liquid water peak.

These observations seem to be in contradiction with the DSC results. However, it can be understood with a closer evaluation in Figure 4. The XRD peaks of hydrated CMK-1-14 at 150 K were fitted by a power law background and 5 Lorentzian peaks. The three sharp peaks were assigned to ice I_h, the broader peak was assigned to ice I_c, and the broadest

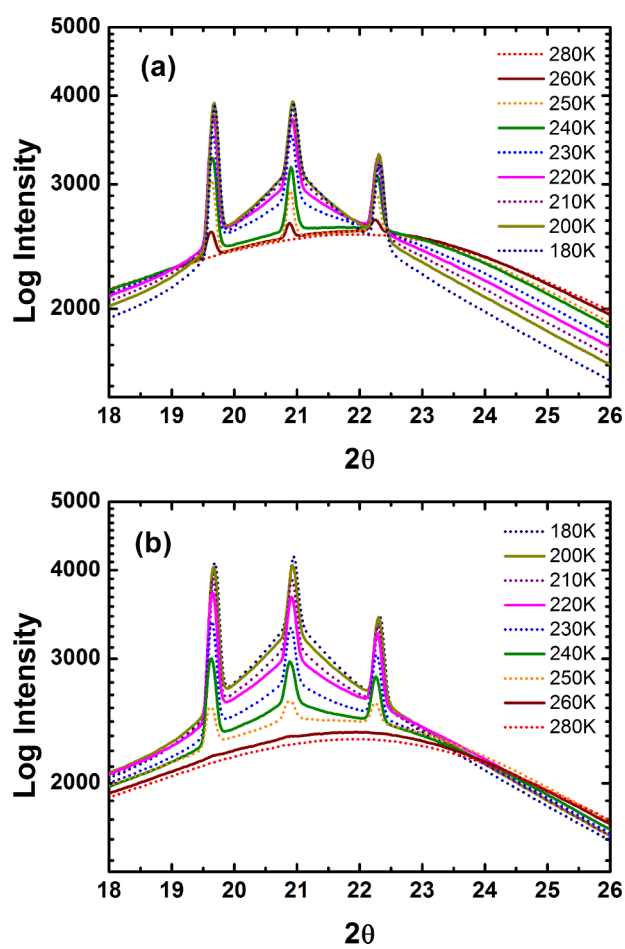

FIG. 3. The *in situ* XRD of hydrated CMK-1-14. (a) Cooling scans. (b) Heating scans.

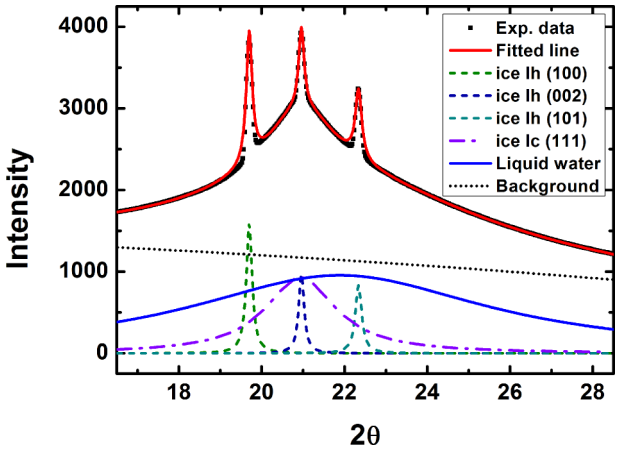

FIG. 4. The XRD of hydrated CMK-1-14 at 150 K. The data were fitted by Lorentz peaks to show ice I_h, I_c, and liquid water exist in the sample.

peak was assigned to liquid water. Without the liquid water peak, the fitting could not converge, indicating the necessity of liquid water existence. Furthermore, the integrated peak intensity of liquid water peak was 77% of the total area, showing that most of the adsorbed water stayed in its liquid form down to 150 K. The sizes of crystalline ice can be estimated by the Scherrer equation,

$$D_p = \frac{K\lambda}{\beta \cos\theta}, \tag{1}$$

where D_p is the average crystallite size, K is the shape factor and chosen to be 0.94, λ is the wavelength of the X-ray, β is the full width at half maximum of the peak, θ is the Bragg angle. The size of ice I_h crystal was about 42.9 nm (average of calculations from the three peaks), and the size of ice I_c crystal was about 3.5 nm. The average size of ice I_h crystal was much larger than the pore size of CMK-1-14, so it can be concluded that ice I_h existed at the inter-particle space of CMK-1-14 grains. The integrated peak intensities of ice I_h were very small relative to the total area, so the freezing and melting of the tiny amount of ice I_h could not be observed in DSC curves. According to the Gibbs-Thomson equation, the ice crystal size as large as 42.9 nm should have freezing and melting temperatures very close to its bulk form, 273.15 K, not at about 230 K as the bumps in DSC curve. At such a slow ramping rate, supercooling effect can be ruled out. Besides, if there was overfilled water outside the pores, they should freeze and melt at a sharply defined temperature, instead of a very wide temperature range. Also with the hydration method used in this study, we should easily avoid over hydrated situations. One explanation may go as follows. A small amount of water was squeezed out of the nanopores because of the density decreasing during cooling. Since the hydration water density gradually dropped, more and more water was expelled out. The fact that ice I_h peaks gradually appeared as temperature changed over a wide range confirmed this explanation. A similar phenomenon has been noticed in the hydrophilic confined water case.[40]

On the other hand, the ice I_c domain size was only slightly larger than the pore size. It is supposed that the ice I_c existed near the opening of pores, where the confinement effect was weak. The freezing and melting of ice I_c may be the origin of the small bumps in the DSC curves (Figure 2). Both DSC and *in situ* XRD results provide evidence that most of the adsorbed water of CMK-1-14 maintained liquid state at the deeply cooled temperature. The peak fitting details and the estimated crystal sizes are listed in Table I.

TABLE I. The peaks fitted by Lorentz function and the crystal sizes estimated by Scherrer equation. Numbers in parentheses are the standard deviation error.

Peak	Center (2θ)	FWHM (2θ)	Area (%)	Size (nm)
Ice I_h (100)	19.700 (0.0008)	0.170 (0.0102)	2.47 (0.088)	42.9 (2.74)
Ice I_h (002)	20.961 (0.0015)	0.158 (0.0114)	1.40 (0.102)	46.3 (3.60)
Ice I_h (101)	22.338 (0.0196)	0.186 (0.0106)	1.42 (0.066)	39.4 (2.38)
Ice I_c (111)	20.939 (0.0114)	2.082 (0.1462)	17.69 (1.601)	3.5 (0.27)
Liquid water	21.884 (0.1084)	8.797 (1.0439)	77.01 (1.857)	

Small angle X-ray scattering (SAXS) curves of hydrated CMK-1-14 at five different temperatures are shown in Figure 5(a). The measured scattering intensity came from two parts. The first part was the scattering from the fractal packing of the CMK grains. Since the CMK grains were at micrometer size, its fractal packing mainly contributed at very low Q range. It came from the scattering length density (SLD) contrast between air and CMK grains. It can be described by a surface fractal law: $I(Q)$ is proportional to Q^{d-6}, where d is the fractal dimension. It is also temperature-independent, so in the log-log scale, it can be fitted as a linear background at all temperatures. The second part was the scattering from the pore-pore

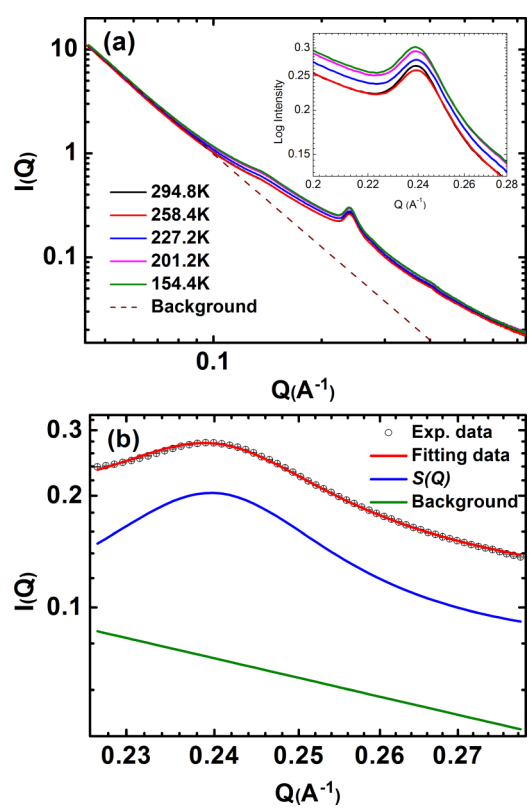

FIG. 5. (a) The SAXS curves of hydrated CMK-1-14 at five different temperatures. The background was fitted by the surface fractal law to the low Q part. The inset enlarges the peak range, so the intensity variation can be clearly shown. (b) The SAXS curve of hydrated CMK-1-14 at 227.2 K. The fitting curve is also shown for comparison.

structure factor peaks, and was more complex due to many intermediate and high-ordered structures. They gave a prominent Bragg peak at Q = 0.24 Å^{-1} and several humps at different Q ranges. These features came from the SLD contrast between carbon matrix of CMK and water inside the pores. In other words, when the average density of confined water changes with temperature, the peak intensity also changes accordingly and thus it can be used to measure the density of confined water. As we have explained above, the other ice phases did not reside in the hexagonally arranged pores and they did not contribute to the intensity of the Bragg peak. The inset of Figure 5(a) shows the enlarged SAXS patterns near the peak at Q = 0.24 Å^{-1}. One can clearly see the intensity change, proofing the extracted density change is a real physical phenomenon, which is independent of the model used in the analysis.

After subtracting the temperature-independent fractal scattering part, the scattered intensity can be represented as

$$I(Q) = C(\Delta\rho^{SLD})^2 S(Q), \tag{2}$$

where C is a constant including the number of scattering units and all other temperature-independent parameters. $S(Q)$ is the structure factor within a grain and gave the peak at Q = 0.24 Å^{-1}, which can be approximated as a Lorentzian function. This function came from the intrinsic broadening factors of instrument and limited size of sample. This part is also temperature-independent. Figure 5(b) shows the SAXS curve of hydrated CMK-1-14 at 227.2 K as an example. The fitting curve is also shown. It is the summation of the Lorentzian part $C(\Delta\rho^{SLD})^2 S(Q)$ and the temperature-independent power law background. The Lorentzian function (Eq. (S1)) used for the fitting and the fitting parameters for each temperatures (Table S1) are listed in the supplementary material.[41] $\Delta\rho^{SLD}$ is the SLD difference between CMK-1-14 and confined water. Since the carbon matrix of CMK-1-14 was rigid and did not change in the temperature range of this study, the SLD of CMK-1-14 can be considered as constant. The scattering intensity of dry sample did not change between 300 and 150 K also supports this assumption. Consequently, all the scattering intensity changes were resulted from the SLD change of confined water, where the SLD has a simple linear relationship to its mass density, ρ^m. It can be represented as $\rho^{SLD} = \alpha\rho^m$, where $\alpha = (b_e N_A \Sigma z_i / M)$, b_e is the scattering length to X-ray of each electron with the value of 2.818 $\times 10^{-13}$ cm, N_A is the Avogadro constant, z_i is the atomic number of the ith atom, and M is the total molecular weight. The mass density of CMK-1-14 was measured as 2.0 g/cm^3 by a helium gas pycnometer. Besides, CMK-1-14 was calcined at 900 °C under nitrogen atmosphere during preparation. There was only trace amount of oxygen (less than 2 wt. % by elemental analyzer) left in the carbon matrix. Following above relationship and assuming that CMK-1-14 was consisted by pure carbon, one can calculate its SLD. After normalizing the calculated water density maximum to the maximum of bulk water density, the density of water confined in CMK-1-14 as a function of temperature can be obtained accordingly.

The extracted average water density is shown in Figure 6, together with the previous SANS measurement of water confined in CMK-1-14,[36] and the SAXS measurement of water confined in hydrophilic nanoporous silica MCM-41-S-15,[38] and the bulk water density[42] before homogeneous nucleation. One notices that the similar trend between the two density curves from SANS and SAXS measurements of water confined in CMK-1-14. Both results show a density maximum at 260 K, 17 K lower than the bulk water, and the density minimum is absent in the measured temperature range. The density maximum at 260 K also concurs with the temperature of ice I_h peaks starting to rise (Figure 3(a)) from the expelled hydration water. The density of water obtained by SANS shows an 18% reduction at the low temperature end compared to density at room temperature. It was suggested that there might be a wetting-dewetting transition that further lowered the average density of water inside the pores. However, as the authors acknowledged, further studies are needed. In the SANS result, the scaling was based on the SLD of heavy water. Since there is no peak observed when CMK-1-14 was hydrated by D_2O, the SLD was assumed to be the same as D_2O due to the contrast matched. This method could lead to some uncertainty in the absolute density of water. However, the calculation from direct measurement of mass density is more reliable in this study. Furthermore, the SAXS technique gives higher flux, higher resolution, and much lower incoherent scattering background. Therefore, we think the result obtained by SAXS is more reliable and reasonable. This can be confirmed again by comparing with the density of water confined in hydrophilic MCM-41-S-15. Although the profile is not exactly the same, which may be due to the surface effect, the density at the lower temperature end is at about the same level. If the density minimum seen in the MCM-41-S-15 case is believed as the full development of a defect-free random tetrahedral network (RTN) of the hydrogen bonds, it should be the lower limit of water density. On the contrary to compensatory interactions that happen at the hydrophilic surfaces, tetrahedral hydrogen bonding pattern is disrupted close to the hydrophobic surface. Because the hydrophobic interaction between the carbon surface and water is relatively unfavorable, there might be a thin depletion layer in between, which gives a lower average density.

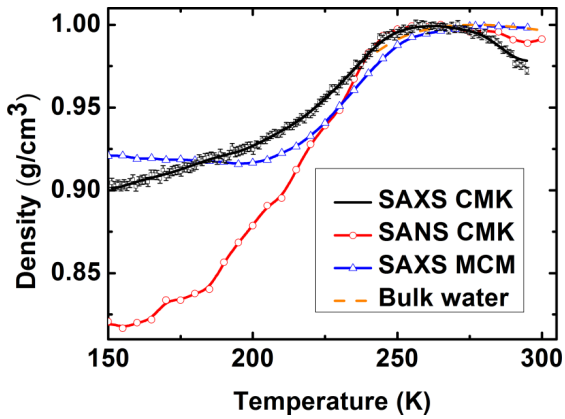

FIG. 6. The average density of water confined in CMK-1-14 as a function of temperature. The SANS measurement of the same sample, and the SAXS measurement of water confined in MCM-41-S-15 are also shown for comparison.

Limmer and Chandler showed that a destabilizing effect that originated from the disordered hydrophilic silica surfaces

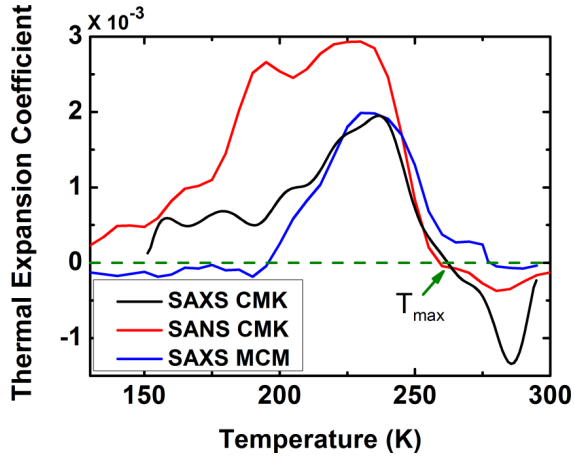

FIG. 7. The deduced thermal expansion coefficient by taking the temperature derivative of the density. The green dashed line is the zero thermal expansion coefficient base line. The green arrow points out the density maximum.

affected the phase behavior of confined water.[43] They further predicted a new phase diagram of hydrophilically confined water, despite intensive debate on the work. However, in our case, the confinement environment is disordered hydrophobic carbon surfaces. It remains to be studied how the disordered hydrophobic surfaces affect the phase diagram of confined water.

Figure 7 shows the thermal expansion coefficient $\alpha_p = (d \ln \rho / dT)$. After taking the temperature derivative, the uncertainty coming from the scaling factor which was used to normalize the obtained hydrophobic confined water density maximum to the bulk water density maximum is removed. The density maximum pointed by the blue arrow appears at the same temperature with both SANS and SAXS techniques. With the updated density profile, the α_p can be deduced more precisely. Instead of a broad peak observed in the previous SANS result, α_p versus temperature shows a sharper peak at $T_L = 235$ K. Therefore, there seems no need to assume a wetting-dewetting transition in such CMK-1-14 hydrophobically confined water. The α_p sharp peak obtained in this work is, however, quite similar to the α_p deduced in the hydrophilic MCM-41-S-15 confinement. Previously, we interpreted the α_p maximum as evidences of crossing of the Widom line,[44] which is generated by the proposed liquid-liquid critical point[45] (LLCP) at elevated pressure. The similar features of the expansion coefficient of water in both hydrophilic and hydrophobic confinement suggest that the maximum α_p temperature may be intrinsic to water, therefore reinforcing the Widom line interpretation.[46]

IV. CONCLUSIONS

In summary, the average densities of deeply cooled water confined in hydrophobic nanopores were measured by analyzing the Bragg peak intensity of SAXS. This result is more reliable than the earlier SANS data. Both the downshift of density maximum to 260 K and the absence of density minimum in the measured temperature range are confirmed. A more reasonable density profile, 10% decreasing comparing to the bulk density at low temperatures, was observed in this study. The deduced thermal expansion coefficient is similar to the hydrophilic confinement case.

ACKNOWLEDGMENTS

The authors appreciate the beam time allocation from National Synchrotron Radiation Research Center in Taiwan, and great helps of beamline managers, Dr. Chun-Jen Su, Mr. Wen-Bin Su, Dr. Yi-Qi Yeh, Dr. Ching-Yuan Cheng, for assisting the setup of experiments. We are grateful to Dr. Wei-Shan Chiang for her profound suggestions. Special thanks to Ms. Jingwei Zhang for reference check and proof reading this paper. The research was funded by Taiwan Ministry of Science and Technology with the project "New Partnership Program for the Connection to the Top Labs in the World".

[1]P. Ball, *Life's Matrix: A Biography of Water* (University of California Press, 2001), available online at http://www.ucpress.edu/book.php?isbn=9780520230088.
[2]D. Chandler, Nature **437**, 640 (2005).
[3]C. Tanford, Science **200**, 1012 (1978).
[4]D. Lucent, V. Vishal, and V. S. Pande, Proc. Natl. Acad. Sci. U. S. A. **104**, 10430 (2007).
[5]Y. Levy and J. N. Onuchic, Annu. Rev. Biophys. Biomol. Struct. **35**, 389 (2006).
[6]W. S. Chiang, E. Fratini, P. Baglioni, D. Z. Liu, and S. H. Chen, J. Phys. Chem. C **116**, 5055 (2012).
[7]E. W. Lang and H. D. Ludemann, Angew. Chem., Int. Ed. Engl. **21**, 315 (1982).
[8]P. G. Debenedetti, J. Phys.: Condens. Matter **15**, R1669 (2003).
[9]J. A. Sellberg, C. Huang, T. A. McQueen, N. D. Loh, H. Laksmono, D. Schlesinger, R. G. Sierra, D. Nordlund, C. Y. Hampton, D. Starodub, D. P. DePonte, M. Beye, C. Chen, A. V. Martin, A. Barty, K. T. Wikfeldt, T. M. Weiss, C. Caronna, J. Feldkamp, L. B. Skinner, M. M. Seibert, M. Messerschmidt, G. J. Williams, S. Boutet, L. G. M. Pettersson, M. J. Bogan, and A. Nilsson, Nature **510**, 381 (2014).
[10]L. S. Bartell and J. F. Huang, J. Phys. Chem. **98**, 7455 (1994).
[11]O. Mishima and H. E. Stanley, Nature **396**, 329 (1998).
[12]P. H. Poole, F. Sciortino, U. Essmann, and H. E. Stanley, Nature **360**, 324 (1992).
[13]L. Liu, S. H. Chen, A. Faraone, C. W. Yen, and C. Y. Mou, Phys. Rev. Lett. **95**, 117802 (2005).
[14]J. C. Palmer, F. Martelli, Y. Liu, R. Car, A. Z. Panagiotopoulos, and P. G. Debenedetti, Nature **510**, 385 (2014).
[15]G. Pallares, M. E. Azouzi, M. A. Gonzalez, J. L. Aragones, J. L. F. Abascal, C. Valeriani, and F. Caupin, Proc. Natl. Acad. Sci. U. S. A. **111**, 7936 (2014).
[16]Y. Liu, J. C. Palmer, A. Z. Panagiotopoulos, and P. G. Debenedetti, J. Chem. Phys. **137**, 214505 (2012).
[17]A. K. Soper and M. A. Ricci, Phys. Rev. Lett. **84**, 2881 (2000).
[18]D. T. Limmer and D. Chandler, J. Chem. Phys. **135**, 134503 (2011).
[19]V. Molinero and E. B. Moore, J. Phys. Chem. B **113**, 4008 (2009).
[20]V. Holten, D. T. Limmer, V. Molinero, and M. A. Anisimov, J. Chem. Phys. **138**, 174501 (2013).
[21]C. A. Angell, M. Oguni, and W. J. Sichina, J. Phys. Chem. **86**, 998 (1982).
[22]R. J. Speedy and C. A. Angell, J. Chem. Phys. **65**, 851 (1976).
[23]C. E. Bertrand, Y. Zhang, and S. H. Chen, Phys. Chem. Chem. Phys. **15**, 721 (2013).
[24]Y. Zhang, A. Faraone, W. A. Kamitakahara, K. H. Liu, C. Y. Mou, J. B. Leao, S. Chang, and S. H. Chen, Proc. Natl. Acad. Sci. U. S. A. **108**, 12206 (2011).
[25]Y. Zhang, A. Faraone, W. A. Kamitakahara, K. H. Liu, C. Y. Mou, J. B. Leão, S. Chang, and S. H. Chen, Proc. Natl. Acad. Sci. U. S. A. **108**, E1193 (2011).
[26]Z. Wang, K. H. Liu, P. S. Le, M. D. Li, W. S. Chiang, J. B. Leao, J. R. D. Copley, M. Tyagi, A. Podlesnyak, A. I. Kolesnikov, C. Y. Mou, and S. H. Chen, Phys. Rev. Lett. **112**, 237802 (2014).
[27]Z. Wang, K. H. Liu, L. Harriger, J. B. Leao, and S. H. Chen, J. Chem. Phys. **141**, 014501 (2014).
[28]N. Giovambattista, P. J. Rossky, and P. G. Debenedetti, J. Phys. Chem. B **113**, 13723 (2009).
[29]X. Q. Chu, A. I. Kolesnikov, A. P. Moravsky, V. Garcia-Sakai, and S. H. Chen, Phys. Rev. E **76**, 021505 (2007).

[30]T. A. Pascal, W. A. Goddard, and Y. Jung, Proc. Natl. Acad. Sci. U. S. A. **108**, 11794 (2011).
[31]M. C. Gordillo and J. Marti, J. Phys.: Condens. Matter **22**, 284111 (2010).
[32]J. Marti, J. Sala, and E. Guardia, J. Mol. Liq. **153**, 72 (2010).
[33]A. Faraone, K. H. Liu, C. Y. Mou, Y. Zhang, and S. H. Chen, J. Chem. Phys. **130**, 134512 (2009).
[34]X. Q. Chu, K. H. Liu, M. S. Tyagi, C. Y. Mou, and S. H. Chen, Phys. Rev. E **82**, 020501 (2010).
[35]R. Futamura, T. Iiyama, A. Hamasaki, and S. Ozeki, Phys. Chem. Chem. Phys. **14**, 981 (2012).
[36]Y. Zhang, K. H. Liu, M. Lagi, D. Liu, K. C. Littrell, C. Y. Mou, and S. H. Chen, J. Phys. Chem. B **113**, 5007 (2009).
[37]D. Z. Liu, Y. Zhang, C. C. Chen, C. Y. Mou, P. H. Poole, and S. H. Chen, Proc. Natl. Acad. Sci. U. S. A. **104**, 9570 (2007).
[38]K. H. Liu, Y. Zhang, J. J. Lee, C. C. Chen, Y. Q. Yeh, S. H. Chen, and C. Y. Mou, J. Chem. Phys. **139**, 064502 (2013).
[39]E. P. Barrett, L. G. Joyner, and P. P. Halenda, J. Am. Chem. Soc. **73**, 373 (1951).
[40]W. A. Kamitakahara, A. Faraone, K. H. Liu, and C. Y. Mou, J. Phys.: Condens. Matter **24**, 064106 (2012).
[41]See supplementary material at http://dx.doi.org/10.1063/1.4929843 for the Lorentzian function (Eq. (S1)) used for the SAXS curves fitting and the fitting parameters at each temperatures (Table S1).
[42]*CRC Handbook of Chemistry and Physics*, edited by W. M. Haynes (CRC Press, 2011), p. 6.
[43]D. T. Limmer and D. Chandler, J. Chem. Phys. **137**, 044509 (2012).
[44]L. M. Xu, P. Kumar, S. V. Buldyrev, S. H. Chen, P. H. Poole, F. Sciortino, and H. E. Stanley, Proc. Natl. Acad. Sci. U. S. A. **102**, 16558 (2005).
[45]K. Stokely, M. G. Mazza, H. E. Stanley, and G. Franzese, Proc. Natl. Acad. Sci. U. S. A. **107**, 1301 (2010).
[46]G. Franzese, G. Malescio, A. Skibinsky, S. V. Buldyrev, and H. E. Stanley, Nature **409**, 692 (2001).